Advances in Science and Technology Research Journal

Advances in Science and Technology Research Journal, 2026, 20(5), 54–74
https://doi.org/10.12913/22998624/215267
ISSN 2299-8624, License CC-BY 4.0

Received: 2025.10.23
Accepted: 2026.03.15
Published: 2026.04.01

Rebar diameter estimation with dual polarised ground penetrating radar

Wiktor Wciślik[1]

[1] Faculty of Civil Engineering and Architecture, Kielce University of Technology, Al. 1000-lecia Państwa Polskiego 7, 25-314 Kielce, Poland
E-mail: wwcislik@tu.kielce.pl

ABSTRACT

This article proposes a procedure for determining the diameter of reinforcing bars in concrete using a dual (cross-polarised) ground-penetrating radar (GPR). Concrete samples were tested with cross-positioned bars of 6, 12, 16, and 20 mm diameters, typically used in construction. Three concrete cover thicknesses were analysed: 35, 50 and 75 mm. Samples were scanned using a GPR with a centre antenna frequency of 2 GHz. It was found that with increasing bar diameter, the mean amplitude of waves polarised in both directions increased linearly. However, consideration of statistical data and amplitude dispersion revealed that the ranges of measured values overlapped in some cases for bars of 'adjacent' diameters, making interpretation of results and diameter assessment difficult. The importance of proper selection of data processing procedures was emphasised, indicating that the highest quality results are achieved by using a bandpass filter and background removal. It was found that, of all the parameters analysed, the most reliable and unambiguous basis for assessing the reinforcement diameter was the quotient of the amplitudes of waves polarised along and across the bar. Even after taking into account the random nature of the results, this parameter allowed for unambiguous differentiation of individual diameters, regardless of the concrete cover thickness. Due to its simplicity and the lack of need for complex data processing, the proposed procedure can be used in practical engineering applications.

Keywords: reinforced concrete structure, non-destructive testing (NDT), rebar, diameter, ground-penetrating radar (GPR).

INTRODUCTION

The long service life and degradation of concrete technical infrastructure necessitate comprehensive and reliable diagnostics. This is crucial not only for operational safety but also for optimal management of funds for repairs, reconstruction, and maintenance.

Non-destructive testing (NDT) methods are currently gaining particular importance, allowing for the inventory of structures, the detection of defects, and the assessment of material parameters without any damage to the structure, sometimes even without interrupting its normal operation.

Various techniques are used in the study of concrete structures, such as: electromagnetic (EM), ultrasonic (UT), radiographic testing (RT), acoustic emission (AE), impact echo (IE), infrared thermography (IRT), drag chain, and others.

Evaluating the diameter of rebar in concrete can also be performed using various NDT methods, each with its own advantages and limitations. The most popular method is electromagnetic locators, which offer quick and simple measurements but only allow for indirect diameter estimation. The accuracy of the results depends on the thickness of the concrete cover. Magneto-inductive techniques offer improved accuracy by analysing the magnetic response of steel. However, the equipment is more expensive than that of electromagnetic locators. Furthermore, interpreting results requires greater qualifications and experience. Pulsed eddy currents or X-ray/CT scanning are characterised by

particularly high accuracy, offering, in addition to rebar identification, the ability to detect corrosion and structural defects. However, the equipment used in these methods is very expensive and inconvenient for on-site use, resulting in very limited application possibilities.

In recent years, the ground-penetrating radar (GPR) method, due to its versatility and non-destructive nature, has become an increasingly popular tool in the diagnosis of reinforced concrete structures. It operates by emitting an electromagnetic wave into the tested medium and recording the wave reflected from objects located within. Therefore, GPR is ideal for inventorying the interior of concrete elements [1, 2], detection of voids and delamination [3, 4], moisture [5–7] and corrosion [8, 9].

From a practical perspective, the flexibility of the method and the portability of the equipment are important. In most cases, on-site inspections pose no practical problems.

One limitation is the inverse relationship between result accuracy and penetration range. The accuracy of 1 cm, typical for engineering applications, requires the use of high-frequency antennas (about 2 GHz), which limits the range to several dozen cm. GPR cannot be used in conductive materials (e.g. metals). In concrete structure testing, a dense reinforcement mesh can be a limitation, causing wave reflection and impeding penetration. GPR results are also very sensitive to environmental factors, primarily moisture.

GPR is characterised by fast data acquisition and high efficiency. However, the equipment is quite expensive. Correct analysis of the results requires extensive experience and is time consuming. Combining all these factors, it can be concluded that GPR falls within the average cost range.

However, despite its numerous advantages, there are still many challenges and unresolved issues hindering the practical application of GPR. One of these is very difficult and unreliable procedure for estimating rebar diameters. This issue is currently the subject of intensive research, but a consistent, reliable procedure is still lacking.

In this paper, an attempt was made to develop a quantitative relationship between the diameter of a reinforcing bar and the selected parameters of the GPR wave reflected from it, taking into account different thicknesses of the concrete cover.

FUNDAMENTALS OF GPR MEASUREMENT

GPR, via a transmitting antenna, emits an electromagnetic wave into the interior of the body being tested (Figure 1). Upon encountering an obstacle (an object with different dielectric properties than the surrounding material, for example, rebar in concrete), the wave is reflected and recorded by the receiving antenna. A local increase in the amplitude of the reflected wave is identified with the presence of an object hidden within the tested medium.

GPR data recording takes various forms. The basic one is a single trace (A-scan, Figure 2a), which represents the relationship between the amplitude of the reflected wave and its bidirectional propagation time (vertical scale). Knowing the wave velocity allows determination of the depth at which the wave was reflected, and thus the depth location of the detected object. Because the

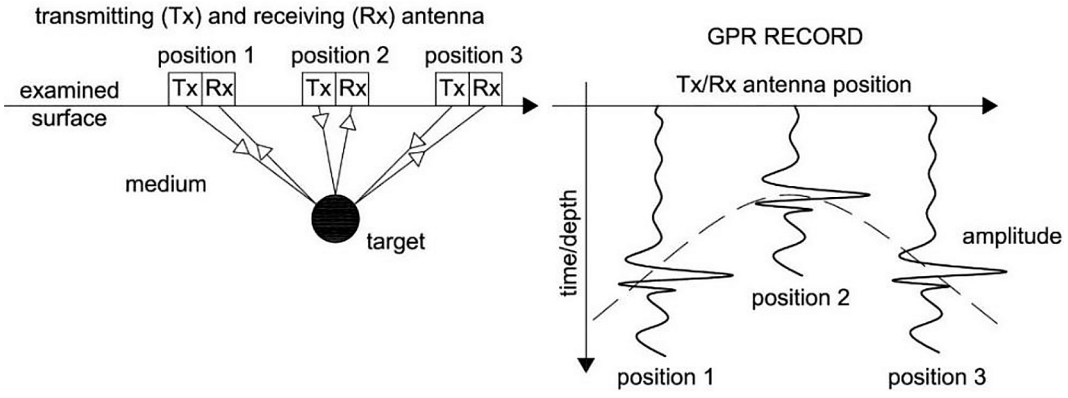

Figure 1. Detection of concealed object using GPR

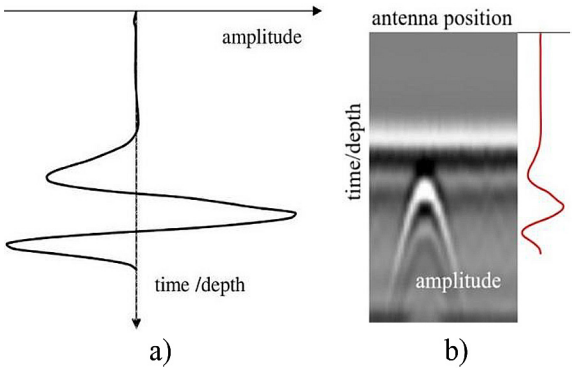

Figure 2. Examples of data recorded by GPR: a) single trace (A-scan), b) radargram (B-scan)

A-scan is the result of a measurement at a point, its usefulness is limited. Another way to visualise the results is a radargram (B-scan, Figure 2b), which is created by combining adjacent A-scans and represents a 'vertical cross-section' of the object being examined along the antenna's path. The upper horizontal axis of the B-scan therefore lies on the body surface, and the vertical axis represents the time scale (converted to depth). Wave amplitude is presented on an adopted colour scale. Figure 2b also shows a characteristic hyperbola, which represents the recording of a wave reflection from a cylindrical object (e.g. a rebar).

REBAR DIAMETER ASSESSMENT WITH GPR – OVERVIEW

The problem of assessing the diameters of cylindrical objects (not only rebars, but also, for example, pipes embedded in the ground) using GPR is not new [10]. One of the first studies in the field of rebar diameter assessment was [11], where, using finite difference simulation and experimental studies, the relationship was established between the amplitude of a wave polarised along and across a rebar, depending on its diameter. It was found that both amplitudes increased linearly with the bar diameter. This effect occurred for all cover thicknesses studied, ranging from 3 to 15 cm. As mentioned, the amplitude ratio is also a good parameter for assessing rebar diameter, as it enables the obtained results to remain independent of the cover thickness and, to some extent, from the dielectric properties of the concrete itself as well as other random factors that are difficult to predict but that affect the measurement result (antenna losses, background noise). Unfortunately, despite performing many measurements, the authors did not provide any measure of the degree of dispersion of the results, which makes it impossible to fully assess the usefulness of the proposed method in practical use.

This approach was developed and analysed by Zanzi and Arosio [12], who emphasised the criteria for selecting the antenna frequency to match the diameter range and the importance of a specific data processing sequence for obtaining high-quality results. Particular attention was paid to careful background removal. Furthermore, it was found that the dependence of the amplitude ratio on the reinforcement diameter determined experimentally sometimes significantly deviates from the theoretical result. The authors indicated the uncertainty regarding the complete removal of noise and interference, the near-field conditions of the measurement, and the impulsive nature of the GPR signal as possible reasons.

The usefulness of the approach based on analysis of two directions of wave polarisation was demonstrated in [13], by examining rebars of different diameters placed at different depths, in different media, and using antennas with different characteristics. As the authors noted, analysis of the energy quotient of reflected signals polarised in two perpendicular directions enabled determination of the rebar diameters with an accuracy of a few percent.

An approximate estimate of rebar diameter using GPR can be made by analysing the amplitude of the wave reflected from the bar, assuming that the amplitude increases with increasing diameter [14]. This method is only approximate, as the amplitude is also influenced by random factors (e.g., physical properties of concrete, varying reinforcement cover thickness), which cannot be completely eliminated during either testing or data processing.

Another method for determining diameters, widely discussed in the literature, is the method of fitting a synthetic (model) hyperbola to a diffraction hyperbola obtained from experimental studies (compare Figure 2b) [15–17]. The shape of the hyperbola (primarily the slope of its arms) depends on the rebar diameter, its depth, and the dielectric constant of the concrete ε_r, which affects the velocity of the propagating wave. The task of determining the diameter therefore comes down to fitting a synthetic hyperbola by optimising the rebar diameter ϕ, depth z and the dielectric constant ε_r in the hyperbola equation. Solving this problem is relatively simple and yields very

accurate results, conditional on high quality of the experimental data and its careful processing [18]. In practical applications, the recorded results are always subject to noise, which remains non-zero even despite the use of filters. This means that the final shape of the hyperbola, in addition to the parameters mentioned above, is also subject to random factors that cannot be completely eliminated. Since the hyperbola optimisation problem is very sensitive to parameter changes, this leads to results that do not reflect physical reality. As shown in [19], a noise level of 2% can lead to diameter estimation errors of up to 500%, which is far from sufficient for engineering applications.

In turn, Ristic et al. [20] pointed out the great importance of careful calibration of wave velocity for precise diameter determination. A two-stage procedure for solving the problem (determining the wave velocity and the rebar diameter, respectively) was proposed by Mechbal and Khamlichi [21]. The crucial importance of accurate determination of wave velocity was also pointed out by Zhan and Xie [22], who also emphasised the usefulness of the stationary wavelet transform (SWT) for determining the rebar diameter. Shihab and Al-Nuaimy [23] observed that imprecise identification of the hyperbola vertex coordinates can result in an error in diameter estimation of up to 50%.

A separate problem of hyperbola fitting, frequently raised in the literature, is the choice of a synthetic hyperbola optimisation method [24]. This issue was discussed, for example, by Dolgiy et al. [25]. To determine the pipe diameter, the authors used weighted least squares, the recursive Kalman filter, the maximum likelihood, the direct least-square fitting, and the Nelder-Mead optimisation. The recursive Kalman filter demonstrated the highest efficiency (average estimation error of 3.06%). Conversely, the direct least-square method yielded the highest error, averaging 15.3%.

The accuracy of diameter estimation is greatly dependent on careful extraction of the hyperbola shape from the recorded radargram. Particular importance is attached to the time zero correction (removing the signal transmitted directly from the transmitting to the receiving antenna and the signal transmitted along the body surface). This allows for the precise determination of the wave propagation time in the tested material and the proper calibration of the curve [24].

The analysis and interpretation of GPR data, including diameter estimation, offer significant potential for the use of artificial intelligence and machine learning algorithms. Recently, Cheng et al. [26] proposed a method using MIMO (multiple input – multiple output) techniques to determine rebar diameters with high accuracy. The procedure involves the use of a linear array of ultra-wideband (UWB) antennas. The obtained results were combined with a diffraction-stacking algorithm to reconstruct the rebar reflection image. The diameter was determined using a 3 dB drop technique. This analysis, conducted on both synthetic and experimental data, allowed the determination of diameters with an error of less than 10%.

Giannakis et al. [27] used neural networks and random forest regression to estimate rebar diameter. Although the network was trained on synthetic data, it enabled accurate estimation based on in situ results. A characteristic feature of the proposed procedure is the use of only a single A-scan for data analysis.

Lei et al. [28], using a convolutional neural network (CNN) and a long short-term memory (LSTM) network, achieved diameter estimation accuracy of 99.5% for synthetic data and 92.5% for field investigation.

In [29], a CNN and the YOLO-v3 (You Only Look Once – version 3) algorithm were successfully used to determine diameters. It was pointed out that the B-scan typically used for analysis is not a sufficiently accurate representation of wave reflection and can only be considered a visualisation method. With small rebar spacing, the arms of adjacent diffraction hyperbolas overlap, which complicates the application of deep learning-based CNN. Therefore, compared to raw data, using data after migration and 'rolling' the hyperbola arms to the vertex provides better accuracy.

In [24] it was pointed out that the problem of hyperbolic overlap becomes significant at bar spacings below 150 mm. However, the authors analysed very small diameters, ranging from 3 to 8 mm. Therefore, it is expected that for larger diameters, the commonly used 12 to 20 mm, the limiting spacing is greater. This means that the phenomenon of hyperbolic overlap is of great importance in interpreting the results of tests on engineering structures.

The deep learning approach was also successfully used in [30]. Among the models used, the YOLO-v8 algorithm was characterised by the highest accuracy (around 97%).

Diameter estimation of cylindrical objects (rebars, pipes) can also be performed using the generalised Hough transform [31, 32]. This method employs the principle of 'voting' individual points of the diffraction hyperbola for a set of geometric parameters of the rebar, which can potentially describe the location of these points. The 'votes' are placed in an accumulator – an array that counts the number of points supporting the proposed parameter sets. The maximum number of 'votes' in the accumulator indicates the most probable set of geometric parameters of the reflector, including its diameter. This method performs well even under significant interference but requires very careful preparation of the input data (e.g. obtaining sharp edges of the radargram).

A separate group of research methods consists of any combination of GPR with other techniques, such as the electromagnetic method [33], which by its nature is more effective in assessing the diameter of bars.

The procedures proposed in the literature are complex, requiring the use of advanced data processing techniques that are not implemented in commercial computer software. Their usefulness in solving practical problems is therefore very limited.

Taking the above into account, this paper attempts to determine the empirical relationship between the diameter of a rebar and selected parameters of the GPR wave reflected from it. Unlike other studies of this type, in this work a statistical analysis of the dispersion of results was performed, which enabled conclusions to be drawn on their unambiguity and the possibility of applying the method in practical engineering. It seems that due to its simplicity, this approach can potentially be a useful tool for solving practical problems.

MATERIALS AND METHODS

Specimens

In order to assess the effect of the rebar diameter on GPR wave parameters, 3 series of concrete samples were prepared as shown in Figure 3. Each series included 3 samples in the form of beams 1250 mm long, 300 mm wide and 150 mm high. Ribbed steel bars with diameters of 6, 12, 16 and 20 mm were concreted perpendicularly to the beam axis, maintaining a constant thickness of the concrete cover in each beam, which was (depending on the sample) 35, 50 and 75 mm.

After concreting, all samples were subjected to a weekly treatment by regularly spraying the surface with water and storing at a constant ambient temperature of 20 °C. After the treatment was completed, the samples were left to dry for 4 months in a laboratory hall, in a dry and warm environment.

As can be seen from the above, all the samples were characterised by the same material properties, and all the differences resulted only from the different thickness of the cover and the diameter of the bar. It should be noted that the described tests were performed in optimal conditions, without taking into account material and environmental factors such as variable concrete moisture, the presence of chlorides, corrosion degradation etc. In engineering practice, these factors occur frequently and significantly affect the results of GPR measurements [9]. The effect of environmental conditions is not discussed here.

GPR stability test

An IDS Aladdin GPR system with 2 GHz centre frequency antenna was used in the study. To ensure quality and repeatability of results, the

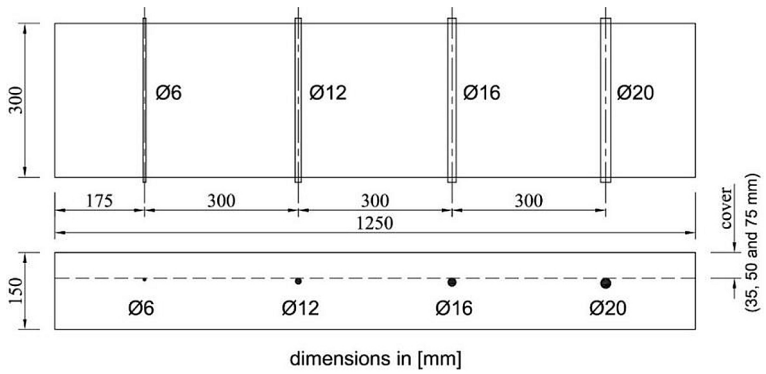

Figure 3. Specimens used in the study

Table 1. Composition of concrete used in the tested samples [9]

Ingredient	Quantity per 1 m³
Portland cement CEM I (42.5 N-MSR/NA)	384 kg
Mine sand	680 kg
Basalt aggregate 2–8	600 kg
Basalt aggregate 8–16	650 kg
Tap water	166 l
Plasticizer ADVA Flow 440 (BV/FM)	0.5% (per 1 kg of cement)
Air entrainer Darex AEAW (LP)	0.2% (per 1 kg of cement)

stability of the GPR apparatus was assessed. The verification was carried out in accordance with ASTM D6087-22 [34]. After starting, the device was allowed to warm up for 20 minutes. After that, 100 waveforms reflected from a metal sheet were recorded. The condition for assessing the stability of the apparatus takes the form:

$$\frac{A_{max} - A_{min}}{A_{avg}} < 0.01 \qquad (1)$$

where: A_{max} – maximum amplitude of wave reflection from metal sheet recorded during the test, A_{min} – minimum amplitude, A_{avg} – average amplitude of all 100 waveforms.

Based on the test, it was found that the condition (1) was satisfied and the GPR device was characterised by sufficient stability [34].

GPR scanning

The actual measurement involved passing the antenna along each sample, on its upper surface (Figure 4). In order to eliminate the effect of wave reflections from the edge of the sample, scanning was performed in two directions. In each direction, scanning was repeated 30 times.

Since the 2 GHz antenna of the Aladdin system is characterised by dual polarisation in two perpendicular directions, the reflections from each rebar were recorded as a wave polarised along the rebar (*L* wave – Figure 5) and perpendicular to it (*T* wave). The result of the measurement for each rebar was therefore the maximum amplitude of the *L* and *T* waves.

During each antenna pass, a radargram was recorded (Figure 6). The results were analysed in two variants: raw data (Figure 6a) and data processed using Gred HD software (Figure 6b). The application of processing procedures was aimed at removing signals that make interpretation difficult (noise, interference, multiple wave reflections from the edge of the sample) and amplifying useful signals (in this case, the wave reflection from the reinforcement bars). For comparison purposes, 2 sets of filters were used: set 1 included move start time (removing the signal passing directly from the transmitter to the receiver, omitting the sample), background removal and linear gain. In set 2 bandpass filter and background removal were used. The selection of filtering methods was preceded by preliminary studies on the impact of the selected method on the quality of the results. Based on this criterion, the above-mentioned sets of filters were selected, after testing bandpass filter, background removal, subtract mean, envelope, linear gain and their different combinations.

Figure 6b shows an example of a radargram processed with set 1. It should be noted, however, that time zero correction affects only the time domain and has no effect on the amplitude values.

(a) (b)

Figure 4. Scanning concrete samples using the IDS Aladdin system and a 2 GHz antenna: a) samples with 3.5 and 5 cm cover, b) sample with 7.5 cm cover

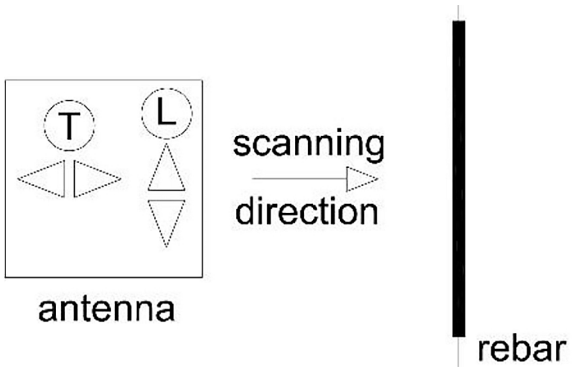

Figure 5. Designations of polarisation directions of the reflected wave

In each case, the analysis was carried out on the values of the maximum amplitude of the *L* and *T* wave reflection from the reinforcing bars, as shown in Figure 7.

As can be seen from above, the *L* and *T* waves were characterised by different polarity. The maximum *L* amplitude was positive (marked in light colours on the radargram – upper diagram in Figure 7). In the case of *T* amplitude (lower diagram), the largest amplitude was negative, which is marked in black.

RESULTS FOR 3.5 CM COVER

Table 2 presents the values of the *L* and *T* amplitudes for bars with diameters from 6 to 20 mm, with a constant cover of 3.5 cm. The results include raw data, amplitudes filtered using set 1 and set 2. In order to present the extent of results dispersion, the table includes standard deviations of all the analysed quantities.

In addition to the values listed in the table, some other statistical parameters were determined. Overall, in all analysed cases, the median values differed very slightly from the mean (no more than 0.01 V), indicating a symmetric distribution and the absence of asymmetric outliers. The coefficient of variation (CoV), depending on the rebar diameter and wave polarisation, ranged from 0.05 to 0.08, so the scatter of the results was relatively small. The relative MAD (the ratio of the median absolute deviation to the mean value) ranged from 0 to 0.05. This indicates that most of the data are less scattered than suggested by standard deviation and the influence of outliers is not dominant. The 95% confidence intervals for the mean amplitudes were relatively narrow (maximum ±4% of the mean amplitude), indicating good estimation precision and low uncertainty associated with the measurement results.

In Figures 8–10, the values from Table 1 are illustrated graphically.

Figure 8a presents the dependence of the amplitude L on the reinforcement diameter (raw data). As can be seen, the amplitude increases monotonically with the increase in the rebar diameter. The amplitude values increase from 1.79 V for 6 mm diameter to 2.76 V for 20 mm bars. Additionally, the graph shows the standard deviation values, indicating the dispersion of the results. The amplitude ranges for 6 and 12 mm bars do not overlap, so the raw data allow these two bars to be clearly distinguished. In the case of larger diameters, there is a clear increase in amplitude with increasing diameter, but high values of the standard deviation cause the amplitude ranges to overlap and thus prevent a clear differentiation of 'adjacent' diameters.

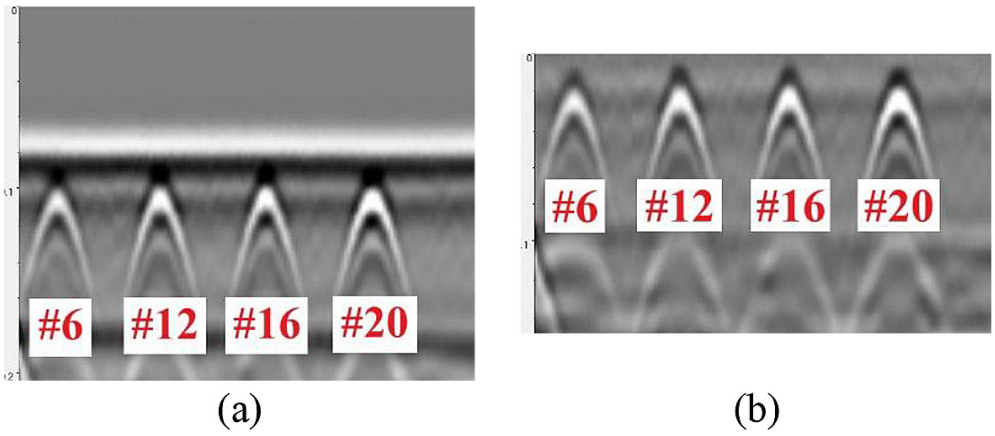

Figure 6. Example of a radargram recorded during tests for *L* polarization: a) raw data, b) data from figure a) after processing with set 1

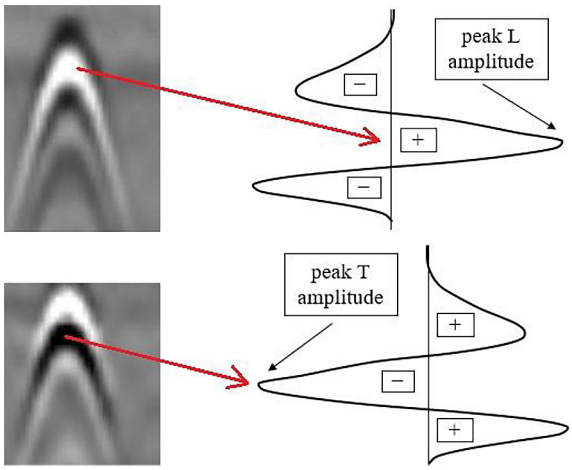

Figure 7. Amplitude of wave reflection from the rebar: amplitude *L* (top), amplitude *T* (bottom)

As mentioned, the raw, unprocessed recording is characterised by noise, which can make analysis and interpretation difficult. In order to remove redundant signals, the amplitudes obtained after processing, using the procedures described above, were also analysed. The use of set 1 (Figure 8b) significantly improved the ability to distinguish between 16 and 20 mm rebars, but at the same time it caused a greater dispersion of results for smaller diameters, thus making the interpretation more difficult. However, the use of set 2 filtration (Figure 8c) did not provide any new information compared to the raw data.

Regardless of the processing procedures used, or lack thereof, due to the overlap in amplitude ranges, the most problematic issue is differentiation of 12 and 16 mm diameters. In each case, there is a strong linear correlation between the amplitude *L* and rebar diameter, as indicated by high values of the R^2 coefficient.

Figure 9a illustrates the same relation for amplitude *T* (wave polarised perpendicularly to the rebar – compare Figure 5). The raw data amplitudes in this case allow for very good differentiation between 6 and 12 mm rebar (the amplitude value was 1.15 V for the 6 mm and 1.92 V for the 12 mm rebar, while the standard deviations were 0.08 and 0.15 V, respectively). Comparing the amplitude values of waves reflected from 12 and 16 mm rebars, it can be seen that although their dependence on the diameter is constantly increasing, the differences are relatively small, which, combined with high values of the standard deviation (0.15 V for 12 mm and 0.20 V for the 16 mm rebar), makes it very difficult or even impossible to practically differentiate these diameters based on the value of amplitude *T* . The difference in amplitudes between the rebars with diameters of 16 and 20 mm is more visible, although the differentiation of these two diameters is not clear.

The use of data processing (within the adopted range – set 1) did not significantly improve the ability to distinguish between diameters, hence these results are not presented here. However, the data quality was significantly improved by using set 2 (bandpass filter + background removal, Figure 9b). Even after including the dispersion of results, amplitude *T* after processing allows for unambiguous differentiation of rebar diameters. However, the differentiation of diameters ϕ12 and ϕ16 may raise some doubts, because, as can be seen in Figure 9b, the ranges of amplitude values overlap to a small extent.

A drawback of estimating the diameter by simple amplitude analysis, however, is the dependence of the amplitude on both the cover thickness and the dielectric properties of the concrete, which in turn depend on its physical properties (e.g. moisture content). To avoid or reduce the influence of these factors, an approach based on the analysis of the quotient of waves polarised in two perpendicular directions was proposed [11, 12].

Table 2. Mean values of *L* and *T* amplitudes, 3.5 cm cover

Parameter	Parameter	Φ6 rebar		Φ12 rebar		Φ16 rebar		Φ20 rebar	
		L [V]	*T* [V]	*L* [V]	*T* [V]	*L* [V]	*T* [V]	*L* [V]	*T* [V]
Raw data	Mean	1.79	1.15	2.17	1.92	2.42	1.99	2.76	2.22
	Std. deviation	0.09	0.08	0.13	0.15	0.24	0.20	0.25	0.18
Processed data (set 1)	Mean	3.99	1.44	4.58	3.53	4.92	3.88	5.66	4.52
	Std. deviation	0.33	0.23	0.38	0.34	0.35	0.32	0.24	0.45
Processed data (set 2)	Mean	1.50	0.17	1.78	0.59	1.82	0.67	2.08	0.88
	Std. deviation	0.11	0.03	0.12	0.05	0.16	0.07	0.15	0.10

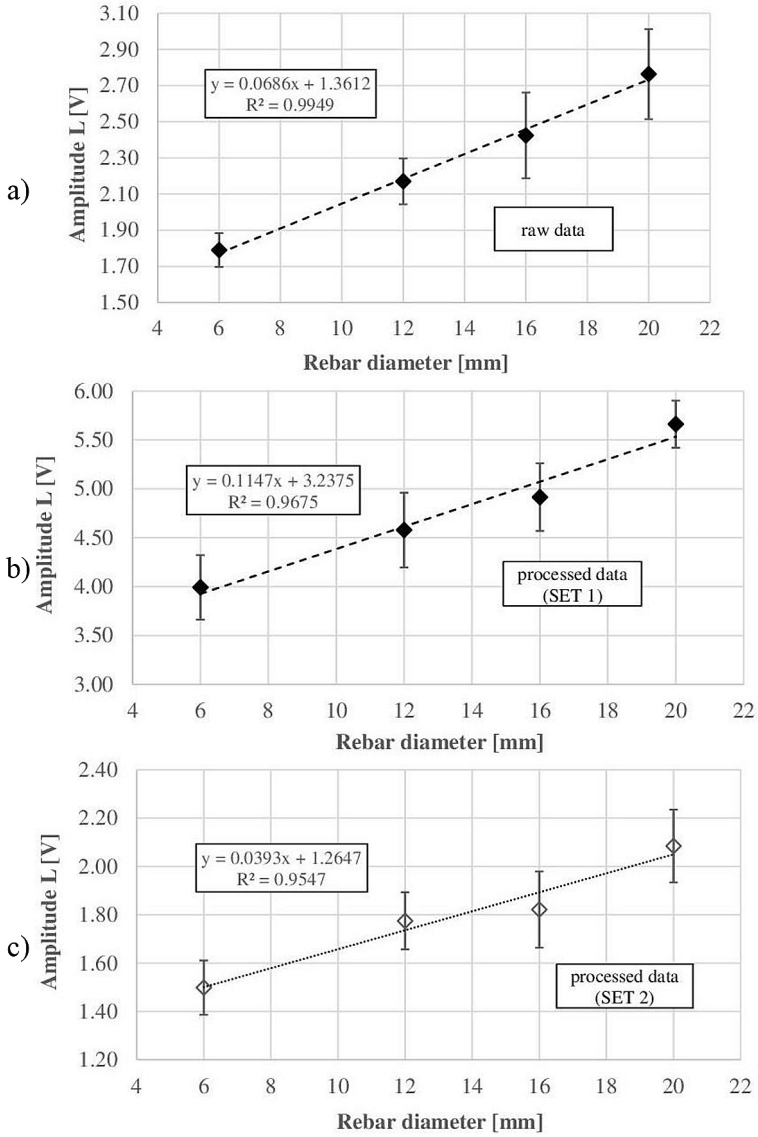

Figure 8. Dependence of amplitude *L* on rebar diameter for a 3.5 cm cover: a) raw data, b) data processed with set 1, c) data after set 2 processing

The graph in Figure 10a presents the relation between the quotient of the *T* and *L* amplitudes and the rebar diameter. As can be seen, both in the case of raw data and those processed with set 1, there is no clear monotonic dependence of the *T/L* quotient on bar diameter. Therefore, the *T/L* value is not useful for assessing the reinforcement diameter. Only in the case of the smallest diameters (6 and 12 mm) does this parameter allow for a clear differentiation.

Much more unambiguous and predictable results were obtained based on data processed using set 2 (Figure 10a). The *T/L* function is increasing over the entire range of analysed diameters, but the slope of the curve is lower than in [11]. In the range of small diameters, the obtained results are convergent, but as the rebar diameter increases, lower *T/L* values were observed than in [11].

Figure 10b shows the same *T/L* relationship (for set 2) along with the standard deviation ranges plotted. As can be seen, the *T/L* value ranges do not overlap, making it easy to distinguish between diameters. As with the raw data and processed using set 1, distinguishing between 6 and 12 mm diameters is the least problematic. However, using set 2 enabled significantly better differentiation of larger diameters than previously.

As can be seen from Figures 8–10, the method of filtering significantly affects the obtained results and the efficiency of determining the diameters. The best quality results are obtained using set 2. However, it is not the effect of a reduction in the

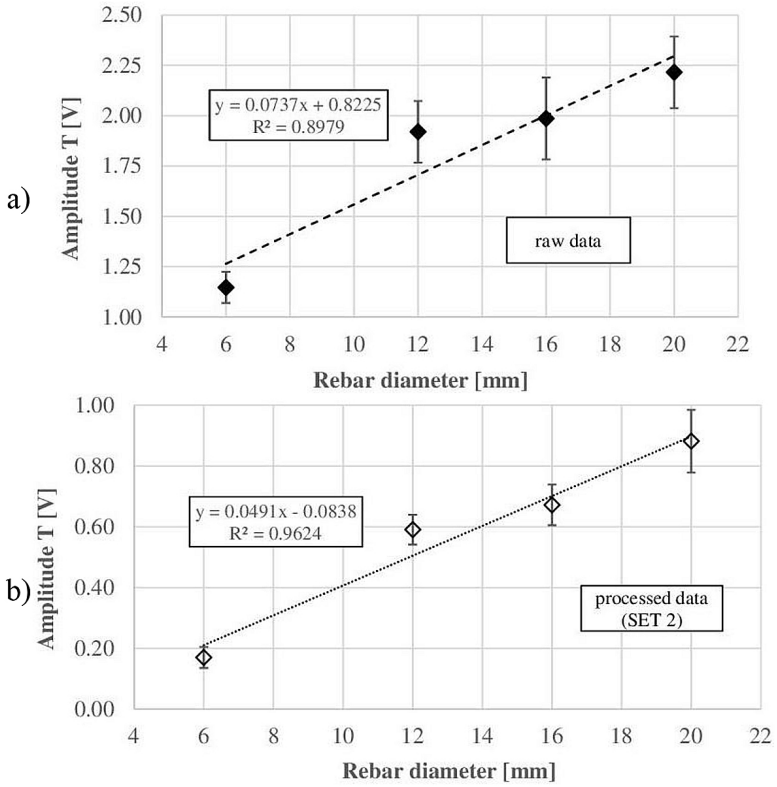

Figure 9. Dependence of amplitude *T* on rebar diameter for a 3.5 cm cover: a) raw data, b) processed data (set 2)

data dispersion after filtering, but rather shifting the mean amplitudes across the adjacent diameters. The change in the mean amplitude after filtering is particularly noticeable for the *T* amplitude, especially in the case of the 6 mm diameter. Before filtering, the mean value was 1.15 V, while after filtering it was 0.17 V. This indicates significant signal noise in the *T* polarisation and a low signal-to-noise ratio. Not surprisingly, this phenomenon is also visible in the *T/L* values.

RESULTS FOR 5 CM COVER

Table 3 presents *T* and *L* amplitude values for a cover of 5 cm. The repeatability of the *L* and *T* amplitude measurement results was similar to that for the 3.5 cm cover. In this case, symmetry in the distribution of results was also observed, manifested by very similar mean and median values. Only in the case of the *T* wave reflected from the 12 mm rebar, the median was approximately 15% lower than the mean, indicating a right-skewed distribution. In the same case, a relatively high coefficient of variation (CoV) of 0.1 was also observed. Apart from that, the CoVs were lower, not exceeding 0.05–0.06. In most cases, the relative MAD (median absolute deviation) oscillated around 0.05, indicating good signal stability. Higher values (of the order of 0.15) were observed for the *T* wave for the 12 mm rebar and both waves reflected from the 20 mm rebar. The obtained 95% confidence interval of ±0.05 indicates good precision of the mean estimation.

Figure 11a shows the dependence of the amplitude *L* (raw data) on rebar diameter. The amplitude values range from 1.56 V for a 6 mm bar to 2.22 V for a 20 mm reinforcement. As before, an increasing, linear dependence of the amplitude on the bar diameter is observed. A high value of the R^2 coefficient, 0.9691, indicates a good correlation between these two quantities. As can be seen from the graph, the amplitude ranges generally do not overlap, which suggests that the bars can be clearly distinguished. As before, the most problematic is differentiation between 12 and 16 mm bars, but the amplitude ranges overlap to a small extent, which potentially allows for a relatively reliable identification of one of these two diameters.

In the case discussed here, data processing with set 1 did not introduce any new information in terms of diameter estimation, hence the processed data are not reported here.

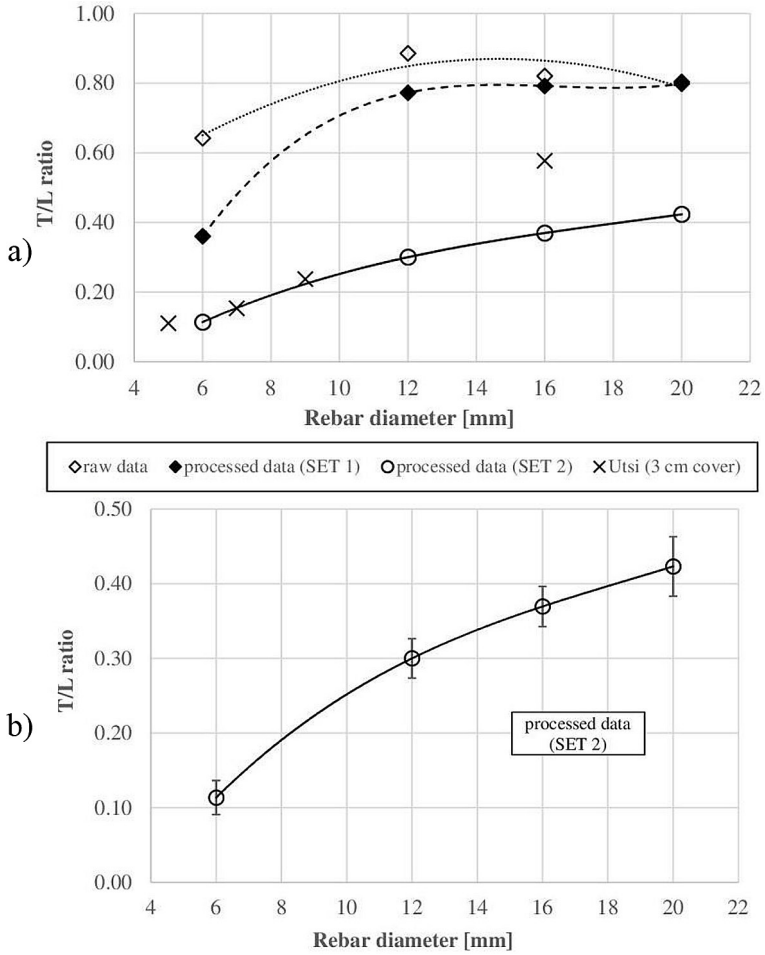

Figure 10. Dependence of the amplitude ratios *T/L* on the rebar diameter, 3.5 cm cover: (a) comparison with literature data, (b) results obtained using set 2 processing

Table 3. Mean values of *L* and *T* amplitudes, 5 cm cover

Parameter	Parameter	Φ6 rebar		Φ12 rebar		Φ16 rebar		Φ20 rebar	
		L [V]	*T* [V]	*L* [V]	*T* [V]	*L* [V]	*T* [V]	*L* [V]	*T* [V]
Raw data	Mean	1.56	0.75	1.77	1.00	1.94	1.10	2.22	1.21
	Std. deviation	0.08	0.06	0.12	0.09	0.10	0.08	0.15	0.13
Processed data (set 1)	Mean	2.34	1.49	3.03	3.43	3.20	3.62	3.42	3.91
	Std. deviation	0.16	0.18	0.37	0.36	0.23	0.27	0.23	0.29
Processed data (set 2)	Mean	1.11	0.22	1.42	0.61	1.51	0.72	1.54	0.85
	Std. deviation	0.07	0.04	0.08	0.05	0.11	0.05	0.10	0.08

The use of set 2 (Figure 11b) for data processing slightly improved the ability to distinguish between 6 and 12 mm diameters. In the 12–20 mm diameter range, the amplitude variation, especially after taking into account the dispersion of the results, was smaller than in the case of the raw data, making the assessment problematic.

Figure 12a illustrates the dependence of amplitude *T* on bar diameter (raw data). Also in this case, a good linear correlation is observed between the amplitude and the reinforcement diameter. The *T* amplitude values change in the range from 0.75 V (6 mm bar) to 1.21 V (20 mm bar). Due to the separate ranges of the amplitudes of the waves reflected from the 6 and 12 mm bars, the differentiation of these diameters based on the T amplitude value is unambiguous. In the range of diameters from 12 to 20 mm, this assessment becomes much more problematic.

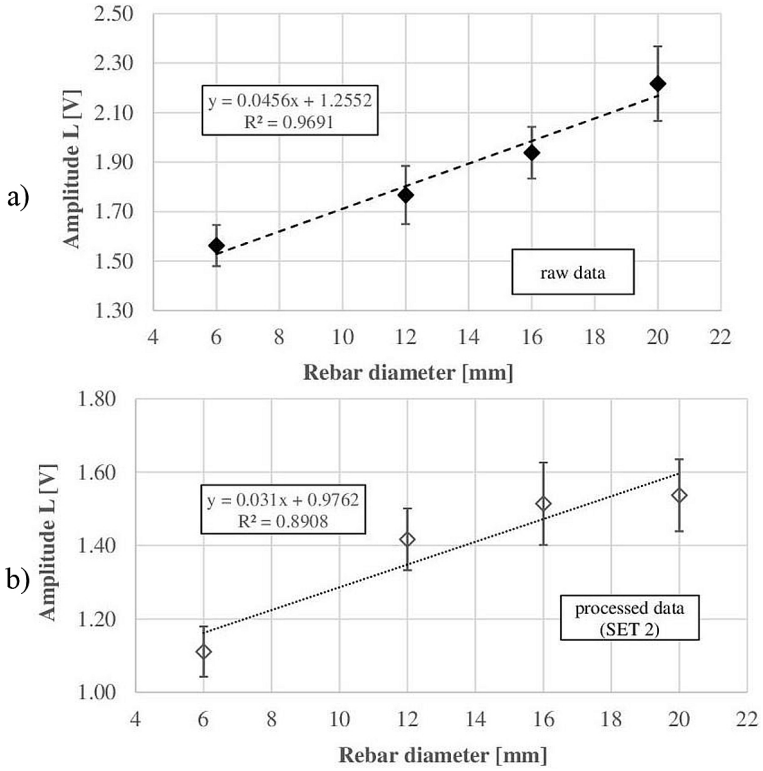

Figure 11. Dependence of amplitude *L* on rebar diameter for a 5 cm cover: (a) raw data, (b) data processed with set 2

The use of set 1 processing did not significantly improve the quality of the result, hence it was not included in this paper. However, processing using bandpass and background removal filters (set 2, Figure 12b) allowed results to be obtained with small dispersion of amplitude values, thanks to which the differentiation of diameters was easy practically in the entire analysed range. The *T* amplitude value increased in this case monotonically from 0.22 V (6 mm diameter) to 0.85 V in the case of 20 mm diameter. Standard deviation ranged from 0.04 to 0.08 V.

Figure 13a presents the dependence of the *T/L* ratio on the reinforcement diameter, both for the raw and processed data. Similarly to the 3.5 cm cover, for raw data and data processed using set 1, no clear dependence was found that would enable the diameters of the reinforcing bars to be determined. A significant difference in *T/L* values was observed only between 6 and 12 mm diameters, but in the larger diameter range, the curves flatten, making it virtually impossible to distinguish between diameters 12–20 mm. Significantly better results were achieved using set 2 for processing. The *T/L* curve increases throughout the entire range of analysed diameters. As before (3.5 cm cover), in the range of small diameters (up to 10 mm), the results obtained here remain consistent with [11]. However, the curve obtained in the study is flatter. This difference is even more visible in comparison to [12], where a significant increase in the *T/L* ratio was observed in the 10–16 mm diameter range. However, it should be remembered that the results from [12] were obtained for a 6 cm concrete cover, not, as in the case discussed here, 5 cm. Furthermore, the differences in results may be the result of different characteristics of the antennas and different parameters of the filters used, as well as different dielectric constants of the concrete [13].

Figure 13b analyses the dependence of the *T/L* ratio on the rebar diameter in more detail, using set 2 filtration (the same data as in Figure 13a). Additionally, standard deviation values are plotted for each case analysed. As can be seen from Figure 13b, even after taking into account the dispersion of results, the *T/L* value ranges do not overlap in any case, making the identification of individual diameters easy. The *T/L* value varied from 0.2 (6 mm diameter) to 0.57 for a 20 mm diameter rebar. Standard deviations ranged from 0.03 to 0.05.

Summarizing the results obtained for the 5 cm cover, the conclusions drawn for the 3.5 cm

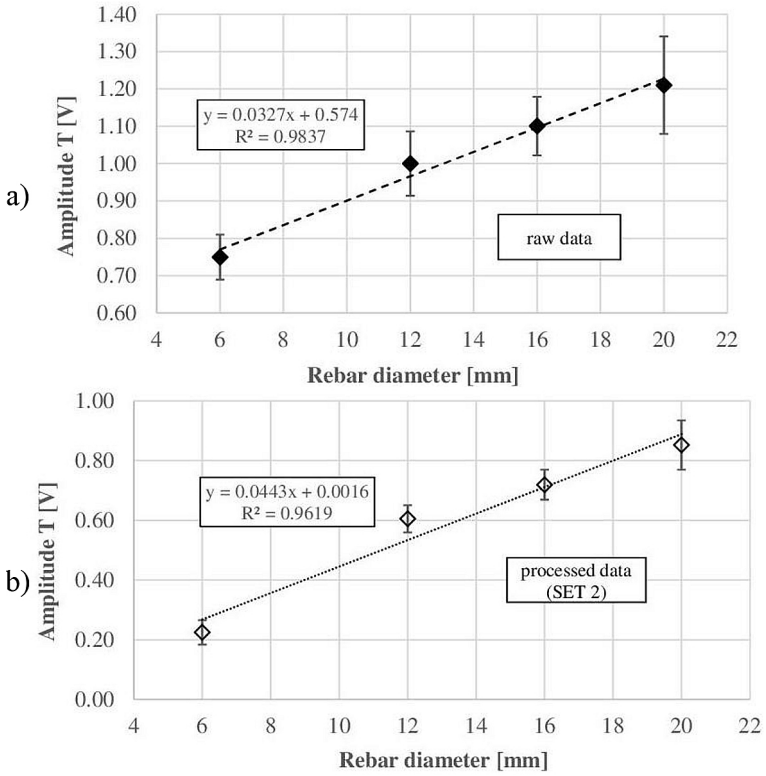

Figure 12. Dependence of amplitude *T* on rebar diameter for a 5 cm cover: (a) raw data, (b) data processed with set 2

cover can generally be confirmed. The use of set 2 significantly improved the diameter resolution by changing the mean amplitude values, especially for the *T* polarisation.

RESULTS FOR 7.5 CM COVER

Table 4 summarizes the mean *L* and *T* amplitudes (with the corresponding standard deviations) for a 7.5 cm cover. The lack of *T* amplitude for the raw data results from significant noise in the unprocessed radargram, which made it impossible to read the peak value. A clear reflection signal from the bars was only visible after filtering.

In the case of the 7.5 cm cover, the dispersion of results is greater than in the previous cases, as evidenced by the coefficients of variation ranging from 0.11 to 0.15. However, the distributions of amplitude values in individual measurements were still symmetrical, which is associated with very similar mean and median values.

Figure 14 summarizes the dependence of amplitude *L* on rebar diameter. Figure 14a illustrates the raw data. The mean amplitude value ranged from 0.76 V for a 6 mm to 1.51 V for a 20 mm diameter rebar. Compared to thinner covers, a weaker linear correlation between the analysed parameters is noticeable. This is likely due to higher attenuation at greater depth, the random nature of wave dispersion, and the probable inhomogeneity of the concrete. As before, applying set 1 filtering did not significantly improve the quality of the results, hence they are not presented here. Set 2 filtering (Figure 14b) significantly improved the correlation. However, compared to the previous covers, the standard deviation values remain high (close to 0.1 V), making practical differentiation between diameters 12–20 mm difficult.

Figure 15 illustrates the relationship between amplitude *T* and rebar diameter. As mentioned above, the considerable noise in the raw data prevented identification of the correct signals, hence only the data after filtering with set 2 are included. As can be seen, both analysed parameters are characterised by a strong linear correlation, but the small variation in amplitude values, along with the significant dispersion in the results, make interpretation and identification of the diameters difficult.

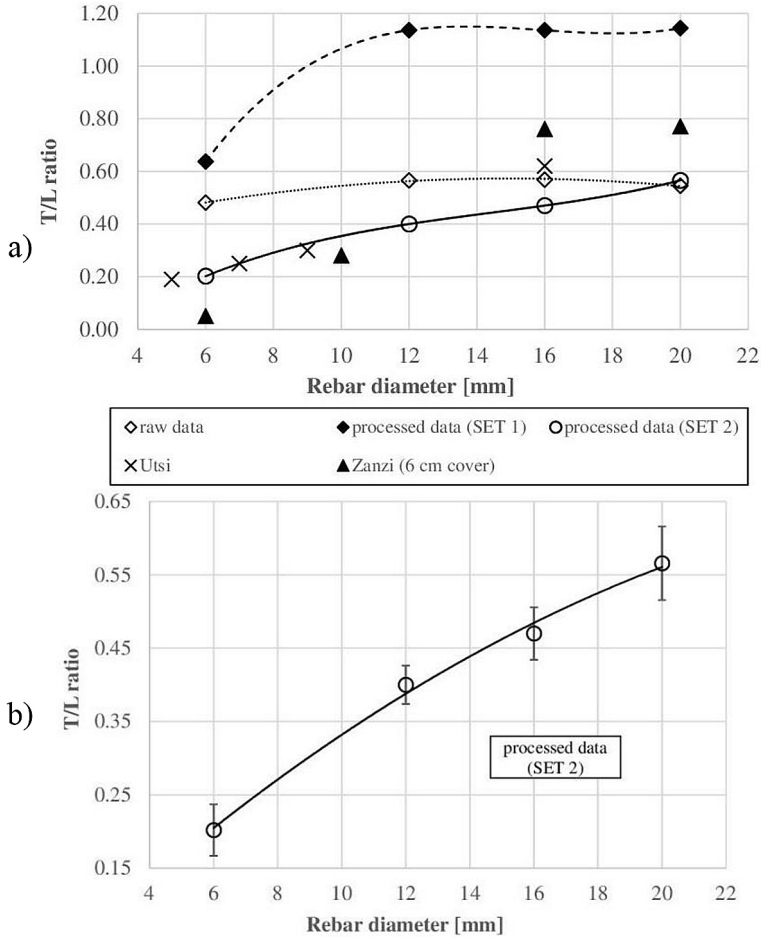

Figure 13. Dependence of amplitude ratios *T/L* on rebar diameter, 5 cm cover: (a) comparison of results with literature data, (b) results obtained using set 2 processing

Table 4. Mean values of amplitudes *L* and *T*, 7.5 cm cover

Parameter	Parameter	Φ6 rebar		Φ12 rebar		Φ16 rebar		Φ20 rebar	
		L [V]	*T* [V]	*L* [V]	*T* [V]	*L* [V]	*T* [V]	*L* [V]	*T* [V]
Raw data	Mean	0.76	-	0.88	-	0.97	-	1.51	-
	Std. deviation	0.10	-	0.13	-	0.11	-	0.17	-
Processed data (set 1)	Mean	1.39	1.22	2.54	2.08	2.75	2.22	3.07	2.42
	Std. deviation	0.12	0.23	0.17	0.35	0.25	0.19	0.22	0.27
Processed data (set 2)	Mean	0.55	0.18	0.78	0.37	0.82	0.45	0.89	0.58
	Std. deviation	0.06	0.05	0.09	0.06	0.08	0.07	0.10	0.08

The graphs in Figure 16 present the dependence of the *T/L* amplitude ratio on the rebar diameter. As before, an increasing relationship between both parameters is visible, being more pronounced in the data after set 2 filtering (Figure 16a). Figure 16b therefore presents this correlation taking into account the dispersion of the results. Although this relationship is very clear, the large dispersion makes it difficult to distinguish a 16 mm rebar from 12 and 20 mm diameter rebars. Overall, the results recorded for the 7.5 cm cover were characterised by lower quality and greater range than previously.

DISCUSSION

Due to wave attenuation in the concrete cover, the amplitude of the wave reflected from the rebar decreases with increasing concrete thickness.

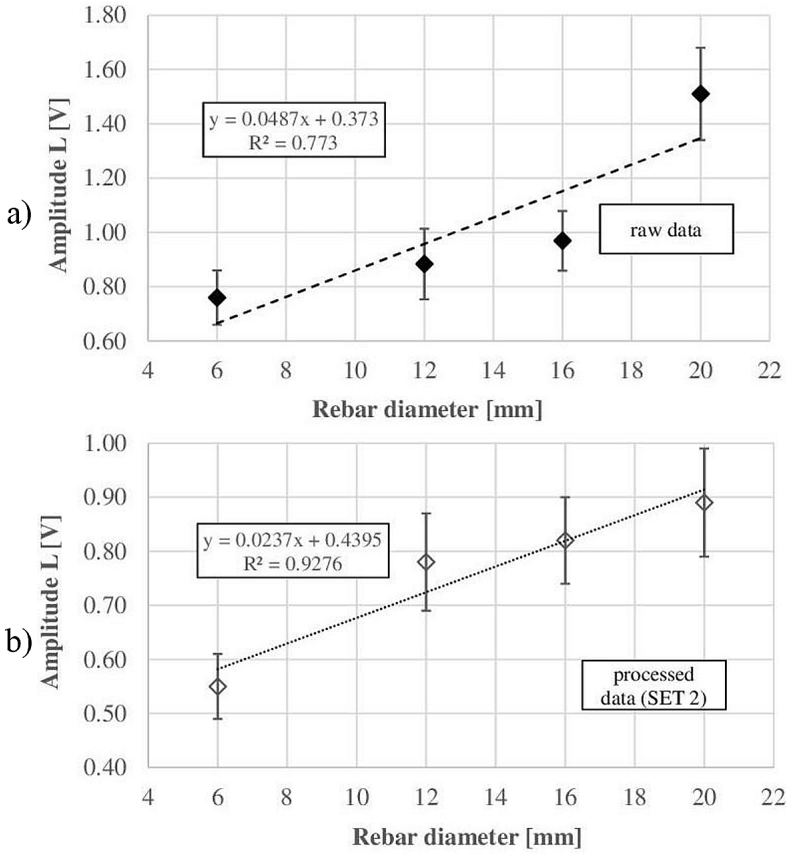

Figure 14. Dependence of amplitude *L* on rebar diameter for a 7.5 cm cover: (a) raw data, (b) data processed with set 2

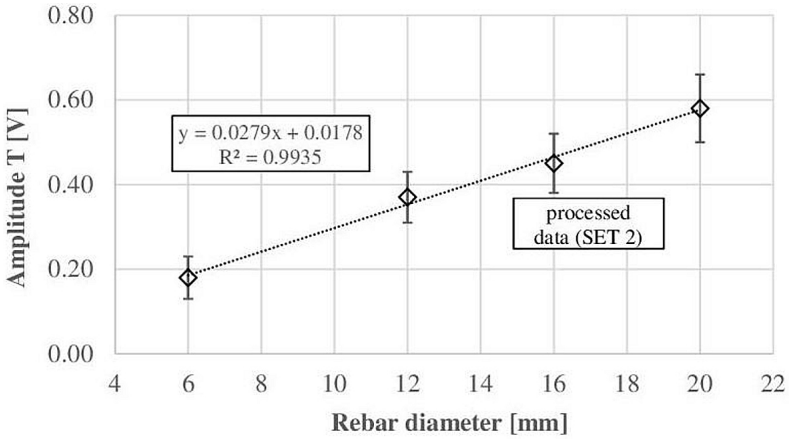

Figure 15. Dependence of amplitude *T* on rebar diameter for a 7.5 cm cover, data processed with set 2

Figure 17 shows an example of the dependence of amplitude *L* on the concrete cover thickness and rebar diameter (data filtered using set 2). As expected, in each case the amplitude decreased with increasing concrete cover thickness.

The relations presented here were also observed for the *T* wave. They were also very similar regardless of the method of processing (set 1 and set 2) or the lack thereof (raw data).

As mentioned above, the *T/L* ratio, regardless of the cover thickness, was well correlated with the bar diameter. Figure 18 illustrates the dependence of the *T/L* ratio on the cover thickness for all analysed diameters, using the set 2 processing. As can be seen, the *T/L* ratio is also sensitive to the cover thickness, so it cannot be treated as a constant value for a given bar diameter. As the cover thickness increased, the *L*

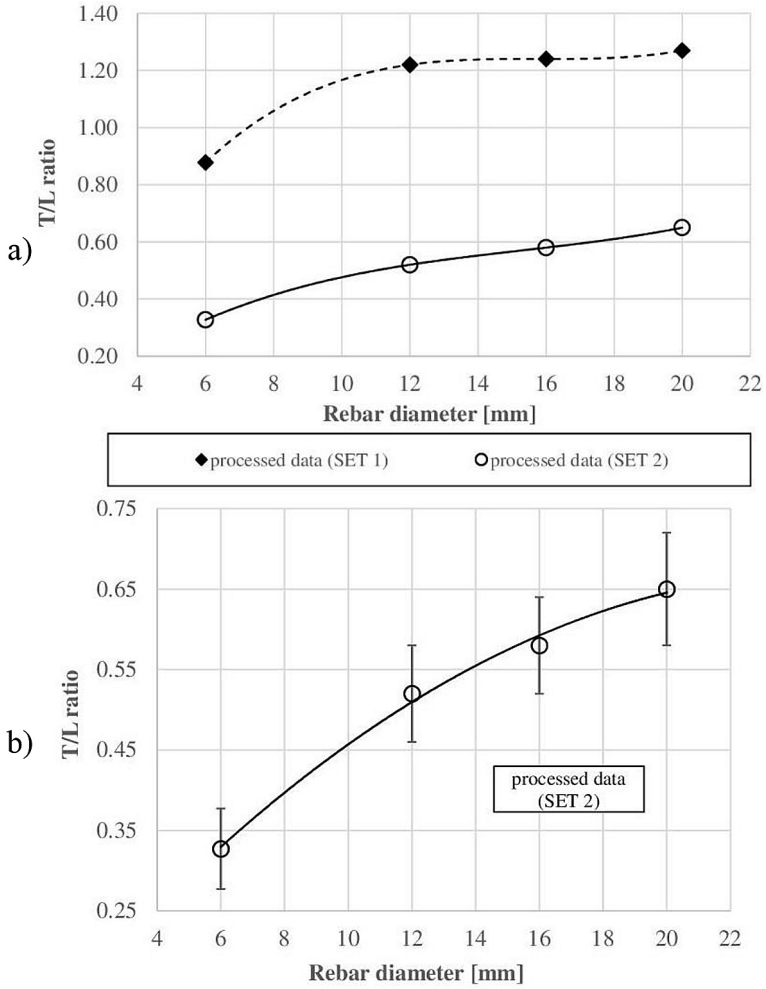

Figure 16. Dependence of the amplitude ratios *T/L* on the rebar diameter, 7.5 cm cover: (a) effect of data processing technique, (b) results obtained using set 2 processing

amplitude value decreased more rapidly. Similar conclusions were described in [11].

It should be noted, however, that the relationships discussed above refer to sound concrete, tested in laboratory conditions without evidence of degradation. Therefore, environmental factors, which undoubtedly significantly influence the analysed parameters, were not taken into account. For example, in bridge structures, moisture and chloride ingress are very common phenomena. As humidity and chloride content increase, wave velocity, as well as the reflected wave amplitude, decrease [5–7], which clearly affects the diameter estimation proposed in this study.

The results presented here are based on medium-strength concrete (C40/50). However, depending on the quality and strength of the concrete, the results may vary [35]. In general, high-strength concretes are characterised by a tight structure and low pore content, which results in low dielectric losses and low wave attenuation. As a result, the amplitude of the wave reflected from the reinforcement is high. Lower-strength concretes, due to their increased porosity, are characterised by higher attenuation and lower wave amplitude. This phenomenon is intensified by severe corrosion and structural degradation of concrete after long-term service.

All the described relationships were determined based on tests conducted in laboratory conditions at temperatures of 20–21 °C. However, significant temperature fluctuations can affect the obtained amplitude values [36]. At high ambient temperatures, lower wave attenuation is observed, which translates into higher amplitudes and a better signal-to-noise ratio. Conversely, at lower temperatures, the amplitude values decrease. However, at subzero temperatures, when the concrete is moist, a significant difference in the dielectric properties of water and ice is also revealed, which in turn results in an increase in amplitude.

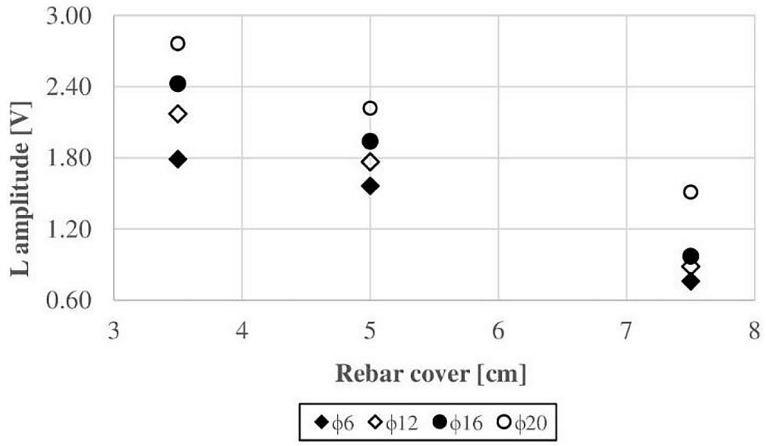

Figure 17. Example dependence of amplitude *L* on cover thickness for the tested rebar diameters, results after set 2 filtration

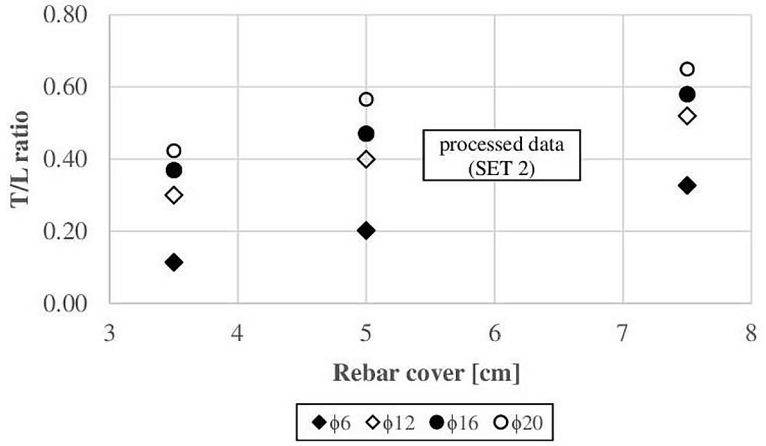

Figure 18. Dependence of amplitude ratio *T/L* on cover thickness for the tested rebar diameters, results processed with set 2 filtration

Although it has not been unequivocally confirmed, it can be generally assumed that the phenomena mentioned above affect the attenuation of both analysed waves (namely, *L* and *T*) to a similar extent. Therefore, it seems that using the *T/L* ratio as a basis for analysis may, to some extent, make the results independent of the environmental factors mentioned above.

The effect of corrosion phenomena is much more complex and has not yet been comprehensively described in the literature. Corrosion of rebar and the surrounding concrete involves several stages, which have different, often opposing, effects on the characteristics of the wave reflected from the rebar [8, 9]. Published papers on this topic provide varying conclusions. Most studies have found that the first stage of corrosion development involves a decrease in wave amplitude as a result of chloride migration within the concrete cover. In the next stage, due to the formation of microcracks and their filling with rebar corrosion products, an increase in wave amplitude was observed as a result of the increasing reflection area. Later stages of corrosion, however, were associated with concrete delamination and debonding at the reinforcement-concrete interface, resulting in stronger wave scattering and a reduction in the amplitude.

However, published studies on the effect of reinforcement corrosion on the parameters of the reflected GPR wave do not describe the phenomenon completely, as experimental studies generally involve artificially accelerated corrosion (electrochemical methods). Therefore, the results do not account for some of the factors that accompany the development of corrosion in structures, such as changes in the structure of the concrete cover caused by cyclic freezing and thawing.

Roughening of the rebar surface by corrosion products also undoubtedly influences the characteristics of the reflected wave.

Therefore, taking into account the possible influence of corrosion phenomena on the parameters of the GPR wave, it is difficult to clearly determine the effectiveness of the proposed procedure in structures with different corrosion advancement.

For comparison purposes, the samples were additionally scanned using an electromagnetic method that employs eddy current induction in the reinforcing bars. A Hilti Ferroscan PS200 device was used for the tests (Figure 19a). According to the manufacturer's guidelines, scanning was conducted on the element's surface in two directions, each time obtaining a tomographic image of the reinforcement structure (Figure 19b).

Diameter measurements were performed using tomographic cross-sections, using software provided by the device manufacturer. The results are presented in Table 5.

Only for the smallest cover did the electromagnetic method enable accurate diameter determination. For the 5 and 7.5 cm cover, the diameter of the 12 mm rebars was overestimated by 16.7%. For the thickest cover, the diameters of the 16 and 20 mm rebars were also incorrect. However, it should be noted that the diameters were determined without calibrating the device on rebars of known diameter.

CONCLUSIONS

The aim of this paper was to assess the diameter of reinforcing bars using the IDS Aladdin georadar and a 2 GHz antenna. Assuming that the amplitude of the GPR wave reflected from the bar increases with the increase in diameter, an attempt was made to develop a quantitative relationship between these two parameters. In contrast to many procedures described in the literature, such an empirical approach is relatively simple, and possible to implement in practical situations without the need for advanced computer software.

The obtained research results clearly indicate the usefulness of the GPR with a 2 GHz antenna for assessing the diameters of reinforcing bars. The basic conclusions include:

- Both the *L* and *T* amplitudes increased significantly with the increase in the reinforcement diameter.

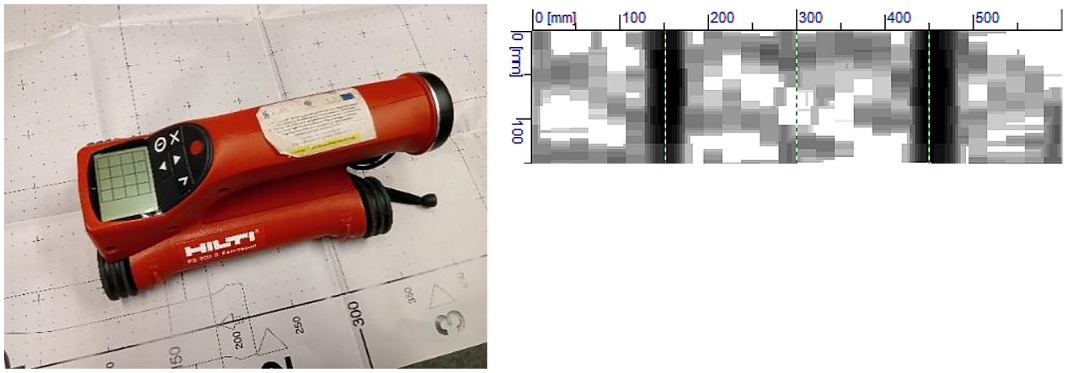

(a) (b)

Figure 19. Measurement using the electromagnetic method: a) Hilti Ferroscan PS200 scanner, b) example of result obtained for 16 and 20 mm rebars at 3.5 cm cover

Table 5. Rebar diameters obtained by electromagnetic method

Parameter	Φ6 rebar		Φ12 rebar		Φ16 rebar		Φ20 rebar	
	Estimated diameter [mm]	Error [%]	Estimated diameter [mm]	Error [%]	Estimated diameter [mm]	Error [%]	Estimated diameter [mm]	Error [%]
3.5 cm cover	6	0	12	0	16	0	20	0
5 cm cover	6	0	14	+16.7	16	0	20	0
7.5 cm cover	6	0	14	+16.7	18	+12.5	22	+10

- The relationship between amplitude and bar diameter was linear, with the best correlation being found for raw amplitude *L*, at cover thickness 3.5 cm.
- The *L* amplitudes obtained from the raw data clearly depend on the rebar diameter. However, after taking into account the dispersion of the results, the ranges of these amplitudes partially overlapped at 'adjacent' diameters, which may lead to error in estimating the diameter. Applying both assumed data processing methods did not improve the clarity of the results.
- Similarly, the *T* amplitude, after taking into account the dispersion of results (raw data), did not allow for a clear identification of diameters in every case. However, the use of bandpass + background removal filtration (set 2) significantly improved the results, making the post-processed *T* amplitude a good basis for estimating the bar diameter, regardless of the cover.
- The most reliable measure for assessing the reinforcement diameter was the *T/L* amplitude ratio, determined from the processed data (set 2). This data enabled unambiguous determination of the rebar diameter for 3.5 and 5 cm cover. For small diameters (up to approximately 10 mm), the obtained results were consistent with the literature data; however, for larger diameters, the *T/L* curve was flatter. This is likely due to the different characteristics of the equipment used and different data processing parameters.
- In the case of a 7.5 cm cover, the *T/L* dependence on the diameter was also clear, but the dispersion of results was greater than before. This means that the identification of larger diameters (12–20 mm) was not unambiguous.
- The *T/L* ratio was not constant for a given diameter but increased with increasing cover thickness. Application of the discussed procedure requires developing and considering *T/L* values for typical cover thicknesses used in concrete structures.

However, some limitations associated with the use of the procedure developed here are mentioned below:

- The developed quantitative relationships are valid only for the GPR system used in the study. In the case of other systems being used, an analogous database should be developed and verified.
- The studies described above concern sound, dry concrete, without corrosion of reinforcement and other destructive factors, such as the presence of chlorides. These factors undoubtedly affect the relations given here.
- The influence of the concrete structure (porosity, type of aggregate, w/c ratio, but also frost degradation and others) on the value of the reflected wave amplitude is unclear.
- The influence of the spacing of reinforcing bars on the possibility of assessing their diameter requires verification.
- The aforementioned analyses assume 2 directions of GPR wave polarization – parallel and perpendicular to the rebar. However, there is no information on the influence of polarisation oblique to the bar axis on the obtained results. This problem may be of great practical importance when scanning atypical elements characterised by a complicated arrangement of reinforcement.

All the above factors will be the subject of further research, which will allow for a more comprehensive assessment of the usefulness of the proposed procedure in practical engineering applications.

REFERENCES

1. Hugenschmidt J., Mastrangelo R. GPR inspection of concrete bridges. Cem. Concr. Compos. 2006; 28: 384–92. https://doi.org/10.1016/j.cemconcomp.2006.02.016
2. Wciślik W. GPR survey of a composite bridge with prestressed concrete beams. In: Proceedings of the 56th Scientific Conference of the Committee of Civil and Water Engineering of the Polish Academy of Sciences and the Science Committee of the Polish Association of Engineers and Technicians, Krynica, Poland, 19–24 September; 2010. (In Polish)
3. Dinh K., Gucunski N. Factors affecting the detectability of concrete delamination in GPR images. Constr. Build. Mater. 2021; 274: 121837. https://doi.org/10.1016/j.conbuildmat.2020.121837
4. Hussein R., Etete B., Mahdi H., Al-Shukri H. Detection and delineation of cracks and voids in concrete structures using the ground penetrating radar technique. J. Appl. Geophys. 2024; 226: 105379. https://doi.org/10.1016/j.jappgeo.2024.105379
5. Kaplanvural I. Volumetric water content estimation of concrete by particle swarm optimization of GPR data. Constr. Build. Mater. 2023; 375: 130995. https://doi.org/10.1016/j.conbuildmat.2023.130995

6. Rodríguez-Abad I., Klysz G., Martínez-Sala R., Balayssac J.P., Mené-Aparicio J. Application of ground-penetrating radar technique to evaluate the waterfront location in hardened concrete. Geosci. Instrum. Method. Data Syst. 2016; 5: 567–74. https://doi.org/10.5194/gi-5-567-2016
7. Hugenschmidt J., Loser R. Detection of chlorides and moisture in concrete structures with ground penetrating radar. Mater. Struct. 2008; 41: 785–92. https://doi.org/10.1617/s11527-007-9282-5
8. Tešić K., Baričević A., Serdar M., Gucunski N. Characterization of ground penetrating radar signal during simulated corrosion of concrete reinforcement. Autom. Constr. 2022; 143: 104548. https://doi.org/10.1016/j.autcon.2022.104548
9. Wciślik W., Raczkiewicz W. Studies on corrosion initiation in reinforced concrete structures using ground-penetrating radar. Materials 2025; 18(10): 2308. https://doi.org/10.3390/ma18102308
10. Hunik R. Detection and sizing of cables and leads with sub-surface radar. In: Proceedings of the 12th World Conference On Non-Destructive Testing. Amsterdam, The Netherlands, April; 1989.
11. Utsi V., Utsi E. Measurement of reinforcement bar depths and diameters in concrete, In: Proceedings of the 10th International Conference on Ground Penetrating Radar. Delft, The Netherlands, June; 2004.
12. Zanzi L., Arosio D. Sensitivity and accuracy in rebar diameter measurements from dual-polarized GPR data. Constr. Build. Mater. 2013; 48: 1293–1301. https://doi.org/10.1016/j.conbuildmat.2013.05.009
13. Sun H.H., Cheng W., Fan Z. Diameter estimation of cylindrical metal bar using wideband dual-polarized ground-penetrating radar. IEEE Trans. Instrum. Meas. 2023; 72: 1–14. https://doi.org/10.1109/TIM.2023.3235447
14. Hasan I. Quantitative non-destructive evaluation of rebar diameter and corrosion damage in concrete using ground penetrating radar. PhD Thesis, The University Of Texas At Arlington, 2015.
15. Fitzgibbon A.W., Pilu M., Fisher R.B. Direct least-squares fitting of ellipses. IEEE Trans. Pattern Anal. Mach. Intell. 1999; 21: 476–80. https://doi.org/10.1109/34.765658
16. Lakshmi K.A., Rahamath A. Estimation of rebar diameter using ground penetrating radar. Int. J. Adv. Sci. Res. Eng. 2017; 3(1): 370–75. https://ijasre.net/index.php/ijasre/article/view/933
17. Lachowicz J., Rucka M. 3-D finite-difference time-domain modelling of ground penetrating radar for identification of rebars in complex reinforced concrete structures. Arch. Civ. Mech. Eng. 2022; 18(4): 1228–40. https://doi.org/10.1016/j.acme.2018.01.010
18. Jaufer R.M., Ihamouten A., Goyat Y., Todkar S.S., Guilbert D., Assaf A., Dérobert X. A preliminary numerical study to compare the physical method and machine learning methods applied to GPR data for underground utility network characterization. Remote Sens. 2022; 14: 1047. https://doi.org/10.3390/rs14041047
19. Giannakis I., Zhou F., Warren C., Giannopoulos A. On the limitations of hyperbola fitting for estimating the radius of cylindrical targets in non-destructive testing and utility detection. IEEE Geosci. Remote Sens. Lett. 2022; 19: 8029005. https://doi.org/10.1109/LGRS.2022.3195947
20. Ristic A.V., Petrovacki D., Govedarica M. A new method to simultaneously estimate the radius of a cylindrical object and the wave propagation velocity from GPR data. Comput. Geosci. 2009; 35: 1620–30. https://doi.org/10.1016/j.cageo.2009.01.003
21. Mechbal Z., Khamlichi A. Determination of concrete rebars characteristics by enhanced postprocessing of GPR scan raw data. NDT&E International 2017; 89: 30–9. https://doi.org/10.1016/j.ndteint.2017.03.005
22. Zhan R., Xie H. GPR measurement of the diameter of steel bars in concrete specimens based on the stationary wavelet transform. e-Journal of Nondestructive Testing 2009; 14(5). https://www.ndt.net/?id=7811
23. Shihab S, Al-Nuaimy W. Radius estimation for cylindrical objects detected by ground penetrating radar. Subsurf. Sens. Technol. Appl. 2005; 6(2): 151–66. https://doi.org/10.1007/s11220-005-0004-1
24. Zatar W., Nghiem H., Nguyen H. Detecting reinforced concrete rebars using ground penetrating radars. Appl. Sci. 2024; 14: 5808. https://doi.org/10.3390/app14135808
25. Dolgiy A, Dolgiy A, Zolotarev V. Optimal radius estimation for subsurface pipes detected by ground penetrating radar. In: Proceedings of the 11th International Conference on Ground Penetrating Radar. Columbus Ohio, USA, June; 2006.
26. Cheng W., Sun H.H., Tan K.H., Fan Z. Estimating the diameter of reinforcing bars using an ultra-wideband MIMO GPR array. Constr. Build. Mater. 2023; 365: 129924. https://doi.org/10.1016/j.conbuildmat.2022.129924
27. Giannakis I., Giannopoulos A., Warren C. A machine learning scheme for estimating the diameter of reinforcing bars using ground penetrating radar. IEEE Geosci. Remote Sens. Lett. 2021; 18(3): 461–65. https://doi.org/10.1109/LGRS.2020.2977505
28. Lei W., Luo J., Hou F., Xu L., Wang R., Jiang X. Underground cylindrical objects detection and diameter identification in GPR B-Scans via the CNN-LSTM framework. Electronics 2020; 9: 1804. https://doi.org/10.3390/electronics9111804
29. Park S., Kim J., Jeon K., Kim J., Park S. Improvement of GPR-based rebar diameter estimation

using YOLO-v3. Remote Sens. 2021; 13(10): 2011. https://doi.org/10.3390/rs13102011

30. Khedr M,, Metawie M., Marzouk M. Integrated ground penetrating radar and deep learning approach for rebar diameter classification in concrete elements. Front. Struct. Civ. Eng. 2025; 19(4): 524–40. https://doi.org/10.1007/s11709-025-1177-4
31. Windsor C., Capineri L., Falorni P., Matucci S., Borgioli G. The estimation of buried pipe diameters using ground penetrating radar. OR Insight 2005; 47(7): 394–99. https://doi.org/10.1784/insi.2005.47.7.394
32. Windsor C.G., Capineri L., Falorni P. A data pair-labeled generalized Hough transform for radar location of buried objects. IEEE Geosci. Remote Sens. Lett. 2014; 11(1): 124–27. https://doi.org/10.1109/LGRS.2013.2248119
33. Zhou, F., Chen Z., Liu H., Cui J., Spencer B.F., Fang G. Simultaneous estimation of rebar diameter and cover thickness by a GPR-EMI dual sensor. Sensors 2018; 18(9): 2969. https://doi.org/10.3390/s18092969
34. ASTM D6087-22 Standard test method for evaluating asphalt-covered concrete bridge decks using ground penetrating radar.
35. Taylor J.M., Morris I.M. Investigating concrete properties using dielectric constant from ground penetrating radar scans. Infrastruct. 2022; 7(12): 173. https://doi.org/10.3390/infrastructures7120173
36. Nguyen T.T., Tung P.T., Tan N.N., Linh N.N., Luc, T.T. A study of factors affecting GPR signal amplitudes in reinforced structures using deep belief networks. Infrastruct. 2022, 7(9): 123. https://doi.org/10.3390/infrastructures7090123